ACS Catalysis

Research Article

pubs.acs.org/acscatalysis

Tailoring Chemical Composition To Achieve Enhanced Methanol Oxidation Reaction and Methanol-Tolerant Oxygen Reduction Reaction Performance in Palladium-Based Nanowire Systems

Christopher Koenigsmann[†] and Stanislaus S. Wong*[,†,‡]

[†]Department of Chemistry, State University of New York at Stony Brook, Stony Brook, New York 11794-3400, United States

[‡]Condensed Matter Physics and Materials Sciences Department, Building 480, Brookhaven National Laboratory, Upton, New York 11973, United States

Supporting Information

ABSTRACT: In this article, we address two key challenges in the development of electrocatalysts for direct methanol fuel cells by rationally tailoring the morphology and chemical composition of Pd-based nanowires (NWs) for enhanced performance. First, we have examined the morphology and composition-dependent performance of $Pt_{1-x}Pd_x$ NWs toward the methanol oxidation reaction (MOR). Elemental Pt NWs were found to possess a significant morphology-dependent enhancement of nearly 3-fold in terms of peak MOR-specific activity over that of commercial Pt NP/C. In addition, tailoring the chemical composition in $Pt_{1-x}Pd_x$ NWs can lead to measurable increases in MOR kinetics, which can be attributed to improved oxidation of formic acid and, potentially, increased selectivity for a direct, CO-free pathway. Second, we have explored the stability of ORR performance in the presence of measurable concentrations of methanol as a function of chemical composition in $Pt_{1-x}Pd_x$ NWs and Pt-free Pd_9Au NWs. In the context of the $Pt_{1-x}Pd_x$ NWs, a distinctive volcano-type dependence has been noted with respect to chemical composition, and on the basis of the MOR activities and methanol tolerant ORR behavior, Pt_7Pd_3 NWs have been highlighted as an optimal catalyst architecture. We have also analyzed the methanol tolerance in Pd_9Au NWs, which represents a highly active, durable Pt-free alternative to traditional Pt-based nanostructured catalysts. Herein, we have demonstrated that Pd_9Au NWs (0.42 mA/cm^2) with no effective Pt content can outperform Pt-based nanostructures, such as Pt NWs (0.32 mA/cm^2) and nanoparticulate Pt NP/C (0.24 mA/cm^2) in the presence of 4 mM methanol/0.1 M $HClO_4$.

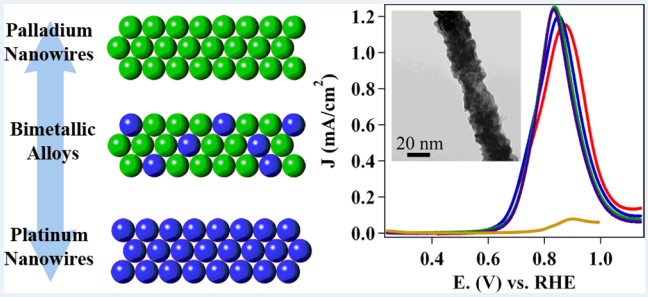

KEYWORDS: *direct methanol fuel cell, formic acid oxidation, one-dimensional morphology, noble metal nanostructure, electrocatalysis*

1. INTRODUCTION

One-dimensional (1D) nanostructures remain the focus of considerable interest as a new and promising structural paradigm for electrocatalysis in polymer electrolyte membrane fuel cells (PEMFCs).[1−6] The distinctive structural and electronic properties associated with 1D nanostructures, such as nanowires (NWs) and nanotubes (NTs), has led to considerable morphology-dependent enhancements in catalytic performance when 1D nanostructures are employed as catalysts.[3,4,7,8] For example, respective enhancements of 7-fold and 2-fold in specific activity toward the oxygen reduction reaction (ORR)[9] and the ethanol oxidation reaction (EOR)[10] have been observed in high-quality, carefully tailored, ultrathin Pt NWs, as compared with state-of-the-art, commercial carbon-supported Pt nanoparticles (Pt NP/C). Similar results have also been noted in the context of the methanol oxidation reaction (MOR) in analogous ultrathin Pt NWs.[11]

Collective experimental results, including electrochemical[9−11] and spectroscopic[11] data as well as theoretical first-principles calculations,[12] have suggested that this distinctive structural and morphology-dependent enhancement emerges from the patently unique anisotropic structure of these materials. Recently, our group,[9,13−18] along with several others,[19−21] has initiated a systematic investigation of the electrocatalytic properties of 1D nanostructures by correlating catalytic performance toward ORR with corresponding trends in the physicochemical properties of the nanowires themselves under study. For instance, significant size-dependent[9,14,15] and composition-dependent[16,22−24] electrocatalytic enhancement has been noted in the performance of noble metal nanowires, including Pt, Pd, and $Pd_{1-x}Au_x$ NWs. In coupling all of these design principles, we have developed a fully optimized, carbon-supported electrocatalyst architecture, consisting of a platinum monolayer shell supported onto an ultrathin Pd_9Au NW core (Pt~Pd_9Au NW), which maintains outstanding specific and Pt-

Received: May 22, 2013
Revised: July 18, 2013
Published: August 8, 2013

   dx.doi.org/10.1021/cs400380t | ACS Catal. 2013, 3, 2031−2040

mass normalized activity values of 0.98 mA/cm^2 and 2.54 A/mg$_{Pt}$, respectively.[3,15]

In addition to the problem of producing highly effective ORR electrocatalysts, two additional, critical challenges have hindered the development of electrocatalysts for practical PEMFCs, employing small organic molecules (SOMs) as fuels.[4,25,26] First, the catalytic oxidation of SOMs, such as methanol and ethanol on noble metals, maintains slow kinetics and often requires high overpotentials as a result of the poisoning effects of carbon monoxide.[27,28] This issue has necessitated the need for high precious metal loadings within the anode of direct methanol fuel cells (DMFCs), for example, thereby limiting their practical commercialization. Considerable work has been expended toward creating 1D nanostructured materials with elemental, bimetallic, and even ternary structures that maintain high activity toward SOM oxidation.[4,29−36] However, despite the breadth of systems investigated, only a few reports have systematically investigated the correlation between chemical composition and the corresponding electrocatalytic performance.[33−35] Second, the problem of methanol crossover from the anode to the cathode in DMFCs is significant and can result in considerable loss of ORR performance due to parasitic oxidation and catalyst poisoning effects.[37,38] In a similar light, the chemical composition of palladium-based nanoparticles has been tailored to achieve considerable improvements in the ORR activity in the presence of SOMs.[38] The incorporation of palladium is uniquely advantageous, since it evinces a relatively high activity toward ORR among the noble metals but is largely inert to the oxidation of MeOH at potentials relevant for ORR.[39−43] Moreover, Pd is more plentiful and significantly less costly than Pt.

Although promising results have been demonstrated in 0D systems, to the best of our knowledge, there have been no systematic reports clearly correlating morphology and composition with the tolerance of ORR activity in the presence of SOMs especially in 1D systems, even though this is an important and practical catalysis issue. This represents a significant endeavor, since many of the intrinsic properties of 1D structures may render them as more active and stable toward catalytic processes in the presence of SOM impurities, which are normally prevalent in actual fuel systems.[4] For example, a consistent increase in the CO tolerance of both Pt and Pd NWs has been observed as their diameters are decreased into the ultrathin size regime.[14]

Therefore, in this report, we undertake for the first time a systematic and rational examination of the MOR performance and methanol-tolerant ORR behavior in high-quality Pd-based nanostructures as a function of both catalyst morphology and NW composition. We have employed a simple, ambient, template-based technique that generates crystalline nanowires with predictable and reproducible control over composition, surface texture, crystallinity, and homogeneity without the need for additional reagents, such as surfactants or other shape-directing agents. In essence, our efforts have focused on the notion of creating a "multifunctional" architecture wherein rationally tuning the physicochemical properties (e.g., morphology, size, and chemical composition) can lead to a single, discrete, and appropriately tailored nanostructured catalyst system that is capable of efficiently and effectively catalyzing multiple types of reactions.[18]

To work toward this goal, we have initially examined the morphology-dependent MOR performance in Pt NWs and demonstrated a significant enhancement of more than 2-fold in the specific MOR activity as compared with state-of-the-art, commercial Pt NP/C. In addition, we have also synthesized a systematic series of alloyed $Pt_{1-x}Pd_x$ NWs with chemical compositions ranging from $1 > x > 0$, including Pt, Pt_4Pd, Pt_7Pd_3, PtPd, and Pd NWs, and the corresponding peak MOR current density has been found to measurably increase as the Pd content is systematically increased toward 50%. Hence, on the basis of CO stripping voltammetry and formic acid oxidation performance in these nanowires, the enhanced activity in the bimetallic nanowires can be ascribed to the addition of Pd, which may facilitate the direct oxidation of methanol through a non-CO pathway.

In the context of methanol tolerance, we have systematically examined the influence of SOMs (in this case, methanol) on the ORR behavior of $Pt_{1-x}Pd_x$ NWs as a function of chemical composition. Interestingly, a volcano-type dependence has been noted with an optimum tolerance to methanol observed in Pt_7Pd_3 NWs, and this trend is clearly distinctive from that found for analogous nanoparticulate catalysts. More importantly, we have also studied the methanol tolerance in highly active Pd_9Au NWs, which were able to retain 88% of their activity in the presence of 4 mM methanol. By contrast, elemental Pt NWs and Pt NP/C possess only 43% and 79% of their initial activity, respectively, in the presence of 4 mM methanol. More importantly, the Pd_9Au NWs sustain an activity of 0.42 mA/cm^2 in the presence of 4 mM methanol, which is measurably enhanced beyond that of the elemental Pt NW (0.32 mA/cm^2) and commercial Pt NP/C (0.236 mA/cm^2) systems, respectively. This interesting and promising result represents a significant advance over our previously reported data[16] and suggests that the Pd_9Au NWs in particular can potentially be employed as highly active and methanol-tolerant ORR electrocatalysts with an activity that exceeds analogous Pt-based catalysts, yet maintains no Pt content whatsoever.

2. MATERIALS AND METHODS

2.1. Synthesis and Characterization of $Pt_{1-x}Pd_x$ and $Pd_{1-x}Au_x$ NWs. The synthesis of high-quality $Pt_{1-x}Pd_x$ and $Pd_{1-x}Au_x$ NWs was accomplished utilizing the so-called U-tube double diffusion technique under completely ambient, seedless, and surfactantless conditions. The experimental details of the synthesis and isolation of elemental and bimetallic NWs are described in great detail elsewhere,[14,16,17] and our discussion herein is necessarily more concise. Specifically, in this synthetic scheme, the NWs are prepared within the spatial confines of a commercial polycarbonate filter membrane. The characteristic tubular pore channels provide for excellent nanosized templates for the subsequent growth of uniform, vertically aligned NWs. A precursor solution and a reducing agent solution held in separate half cells are introduced into the template pores by means of double diffusion, thereby resulting in the nucleation and growth of crystalline nanowires. Chemical composition control is readily achieved by manipulating the relative fraction of the desired precious metal salts (e.g., $HAuCl_4$, H_2PtCl_6, or Na_2PdCl_6) in the presence of a precursor feed solution, which generates a corresponding nanowire of identical composition. Either individual NWs or free-standing, vertically aligned NW arrays can be isolated by either dissolving the template membrane in dichloromethane or decomposing the template matrix in an argon plasma environment.

The characterization of the growth mechanism, purity, crystallinity, composition, homogeneity, and structure of the NWs has been described in detail in prior reports.[4,14,16] In short, the as-prepared NWs consist of the pure face-centered cubic phase of either elemental Pd or Pt or the bimetallic $Pt_{1-x}Pd_x$ or $Pd_{1-x}Au_x$ alloy phases. This chemical composition has been characterized in detail by energy-dispersive X-ray spectroscopy (EDAX) and X-ray diffraction analyses, which confirm that the chemical composition of the NW is essentially determined by the contents of the precursor solution and that all samples maintain the desired homogeneous alloy-type structure. In addition, we have demonstrated by high-resolution TEM (HRTEM) that these as-synthesized Pd NWs and Pd_9Au NWs are not only essentially single-crystalline but also highly textured, whereas their $Pt_{1-x}Pd_x$ counterparts maintain oriented polycrystalline structures. The surfaces of the nanowires are highly faceted, and the sizes and shapes of the facets are determined by the roughened interiors of the template pores. All NWs within this report possess a diameter of 50 ± 9 nm. Hence, the chemical composition of the NWs has been highlighted as the key parameter in determining their electrochemical properties.

2.2. Electrochemical Experiments. The electrochemical measurements were conducted with the as-prepared catalysts, supported onto a 5 mm glassy carbon rotating disk electrode (GCE) polished to a mirror finish. The deposition of a desired NW sample was accomplished by first pre-modifying the surface of the electrode with a thin layer of carbon by drop-casting two 5 μL drops of 1 mg/mL solution of Vulcan XC-72R carbon, dispersed into 25% isopropyl alcohol in water, onto the surface of the electrode, followed by rapid drying under vacuum. The modified electrode was then loaded with the respective NW sample by placing one 5 μL drop of a ∼1 mg/mL solution of the NWs onto the surface and allowing the solvent to dry under ambient conditions. In the case of the Pt NP/C, the commercial powder, consisting of 20% Pt NPs supported on Vulcan XC-72R (BASF), was dispersed into 25% isopropyl alcohol in water at a concentration of 2 mg/mL. The electrode was modified with the Pt NP/C by drop-casting one 5 μL drop of the dispersion onto the surface of the bare GCE, which was then dried rapidly under vacuum. The dispersion of the catalyst was examined by optical microscopy to ensure a homogeneous distribution of the catalyst onto the GCE surface. Subsequently, all electrodes were sealed with 1 drop of 0.025% solution of Nafion dissolved in ethanol, prepared from a 5% stock solution (Aldrich).

The pre-modification of the GCE surface has been previously demonstrated to be useful in approximating the textured carbon surfaces within practical functional devices and can also contribute to an improved distribution of nanowires over the geometric area of the electrode;[14,16] however, the addition of carbon to the electrode is not really necessary to promote a uniform distribution of the individual isolated NWs, as homogeneous dispersions of nanowires can be achieved directly on the GCE surface itself.[14] Since the carbon maintains essentially no catalytic activity toward either MOR or ORR by comparison with the noble metal catalysts themselves, the comparison of the performance of $Pt_{1-x}Pd_x$ and $Pd_{1-x}Au_x$ NWs supported on a porous carbon substrate with that of Pt NP/C has been widely employed in the existing literature.[1−4,6]

Prior to electrochemical experiments, our as-prepared electrodes were immersed in ultrapure water (R = 18.2 MΩ·cm) to remove residual impurities and salt residues. Electrochemical experiments were conducted utilizing a three-electrode setup within a custom-made glass electrochemical cell. A silver/silver chloride (Ag/AgCl) electrode housed in a double junction chamber (BASi) and a platinum foil served as the reference and counter electrodes, respectively. These experiments were performed in a 0.1 M $HClO_4$ electrolyte, prepared by diluting a concentrated solution (Fisher Scientific, Optima grade) in ultrapure deionized water. All potentials are reported with respect to the reversible hydrogen electrode (RHE) unless otherwise specified.

Cyclic voltammetry (CVs) and CO stripping voltammetry data were collected in argon-saturated 0.1 M $HClO_4$ at a scan rate of 20 mV/s. Prior to CO stripping, the electrode was immersed in a CO-saturated 0.1 M $HClO_4$ solution for a period of 30 min to ensure complete adsorption. The electrode was then transferred directly to the argon-saturated electrolyte for CO stripping experiments. The catalytic MOR and formic acid oxidation reaction (FAOR) performances were measured by obtaining linear sweep voltammograms (LSVs) in the anodic sweep direction in a solution consisting of either 0.1 M methanol (Fisher Scientific, Optima grade) or 0.1 M formic acid (Fisher Scientific, Optima grade), respectively, supported in a 0.1 M $HClO_4$ electrolyte at 20 mV/s. The electrochemically accessible surface area (ESA) was calculated from the integrated hydrogen adsorption, determined in the cyclic voltammetry analysis, utilizing 0.21 mC/cm^2 as the conversion factor. Although the use of the hydrogen adsorption charge may result in a slight overestimation of the ESA due to the additional effect of hydrogen absorption in Pd, we have previously demonstrated by means of CO stripping and Cu underpotential deposition that the ESA determined by hydrogen absorption is consistent with these methods and that any deviations are within experimental variation.[14] In addition, we have selectively employed the hydrogen adsorption process so as to obtain an ESA that is related only to the number of Pd active sites in the Pd_9Au NWs, since the Au atoms do not undergo underpotential deposition of hydrogen. Essentially, we have selected this method so that useful comparisons can be made between the Pd active sites of elemental Pd NWs and those of bimetallic Pd_9Au NWs without the contribution of the Au atoms, which are essentially catalytically inert. Additional details can be found in prior reports.[15,16,18]

The ORR activity was measured, utilizing the thin-layer rotating disk method described in detail by Kocha and co-workers.[44] Specifically, polarization curves were obtained in the anodic sweep direction in oxygen-saturated 0.1 M $HClO_4$ at a rate of 10 mV/s with the electrode rotating at 1600 rpm. The kinetic current was measured at 0.9 V using the Koutecky−Levich equation and was normalized to the ESA to yield an area-normalized kinetic current density or so-called specific activity. The methanol tolerance was examined by obtaining a series of polarization curves in electrolytes with increasing methanol concentrations. In the case of the commercial Pt NP/C and $Pt_{1-x}Pd_x$ NWs, separate polarization curves were obtained in 0.1 M $HClO_4$ electrolytes containing methanol concentrations of 0, 1, 2, 3, and 4 mM, respectively. In the case of the highly methanol-tolerant Pd and Pd_9Au NWs, polarization curves were obtained in 0.1 M $HClO_4$ solutions containing methanol concentrations of 0, 1, 2, 3, 4, 25, 50, 75, and 100 mM, respectively. The relative methanol tolerance was estimated by normalizing the measured specific activity in the presence of methanol (J_K [MeOH]) to the measured specific

dx.doi.org/10.1021/cs400380t | ACS Catal. 2013, 3, 2031−2040

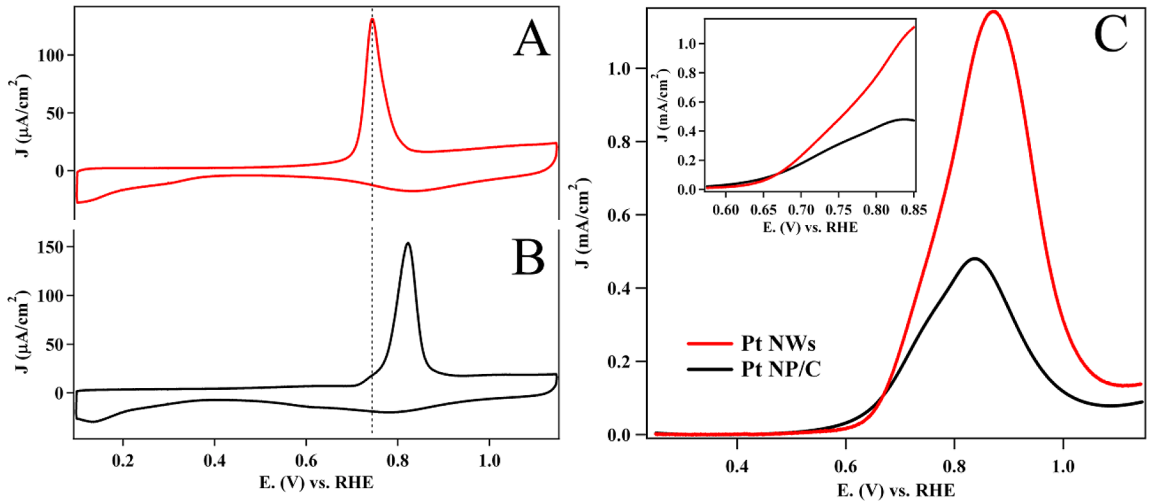

Figure 1. Representative CO stripping voltammograms obtained from Pt NWs (A) and commercial Pt NP/C (B). The dashed line highlights the potential of the CO stripping peak in the Pt NWs. The morphology-dependent methanol oxidation performance is characterized by LSVs obtained in 0.1 M methanol (C) with the onset region of the LSV, highlighted in the inset.

activity in a pure solution containing no methanol (J_K). The measurement of the fraction of specific activity in the presence of methanol with respect to the activity in a pure electrolyte (i.e., J_K [MeOH]/J_K) provides for a useful metric of the level of methanol tolerance as a function of NW composition.

3. RESULTS AND DISCUSSION

3.1. Morphology-Dependent Enhancement of MOR Activity in Anisotropic Pt NWs. To demonstrate the inherent advantages of our as-prepared NWs, we systematically examined the morphology-dependent electrocatalytic performance toward MOR in elemental Pt NWs. The measured MOR currents obtained from LSVs in the presence of 0.1 M methanol for Pt NWs and Pt NP/C were normalized to the ESA of the respective catalysts so as to provide for area-normalized LSVs, shown in Figure 1C. Interestingly, the Pt NWs displayed a nearly 3-fold higher MOR peak current density, as compared with the Pt NP/C. In addition, a careful inspection of the MOR onset region, shown as an inset to Figure 1C, reveals that the Pt NWs and Pt NP/C maintain comparable onset potentials of ∼675 mV; however, the Pt NWs possess higher overall MOR kinetics after onset by comparison with the Pt NP/C. Collectively, all of these results demonstrate a significant and measurable morphology-dependent enhancement behavior in MOR performance, which likely can be attributed to the 1D Pt NWs themselves.

The mechanism of MOR on Pt, although it is highly complex, is believed to occur in two primary steps, with CO representing a key intermediate.[45] First, adsorbed methanol on the surface of Pt is thought to undergo a rapid dehydrogenation process leading to the adsorbed CO intermediate. The subsequent oxidation of the CO intermediate proceeds relatively slowly at potentials close to the thermodynamic potential as a result of a lack of adsorbed oxygen species, such as Pt−OH*, which are believed to facilitate the oxidation process.[46] In essence, the high coverage of CO at low potentials results in a poisoning effect and blocks effective MOR catalysis at the Pt active sites. The issue of CO poisoning on Pt nanostructures has been addressed by introducing small quantities of more oxophilic metal species, such as Ru and Sn, which would facilitate a bifunctional mechanism.[27]

In this case, however, we have demonstrated that it is feasible to increase the MOR kinetics by simply tailoring the morphology of the Pt catalyst itself. Specifically, CO stripping voltammograms obtained from the Pt NWs and Pt NP/C highlight a significant shift in the CO stripping peak potential of nearly 80 mV to lower potentials in the Pt NWs (Figure 1A), especially as compared with analogous Pt NP/C (Figure 1B). The improvement in CO stripping kinetics in the Pt NWs suggests that the 1D morphology facilitates CO oxidation at lower potentials. This phenomenon has been observed previously in ultrathin Pt NWs, and is believed to arise from the unique electronic properties associated with the 1D morphology.[10,11] Specifically, Guo and co-workers[11] have demonstrated that the significantly improved CO kinetics may arise from a shift in the weighted center of the d-band as a result of the observed anisotropic structure and nanosized diameter, which may lead to weaker interactions between the Pt surface sites and the CO adsorbate.

3.2. Composition-Dependent Performance in $Pt_{1-x}Pd_x$ NWs with Homogeneous Alloy-Type Structures toward the Methanol Oxidation Reaction and the Formic Acid Oxidation Reaction. Recently, several reports have focused on the homogeneous $Pt_{1-x}Pd_x$ alloy as a promising bimetallic system with direct and practical application as both highly active MOR electrocatalysts and as methanol-tolerant ORR electrocatalysts. For example, in our prior work, we tailored the chemical composition of $Pt_{1-x}Pd_x$ NWs and examined the composition-dependent performance toward ORR. Herein, we move beyond our previous study by rationally examining the potential for these 1D bimetallic catalysts to serve as multifunctional catalysts with high performance toward MOR and ORR. In this section, we have systematically investigated the electrocatalytic MOR and FAOR performance as a function of chemical composition.

Toward this goal, LSVs were obtained in 0.1 M methanol, supported in 0.1 M $HClO_4$ from Pt, Pt_4Pd, Pt_7Pd_3, and PtPd NWs. These curves are shown in Figure 2A. First, the Pt and Pt_4Pd NWs maintained an onset potential that is ∼25 mV lower than that of the corresponding Pt_7Pd_3 and PtPd NWs. The lower onset potential in the Pt-rich NWs is likely a result of the larger number of Pt sites at the catalytic interface, which

dx.doi.org/10.1021/cs400380t | ACS Catal. 2013, 3, 2031−2040

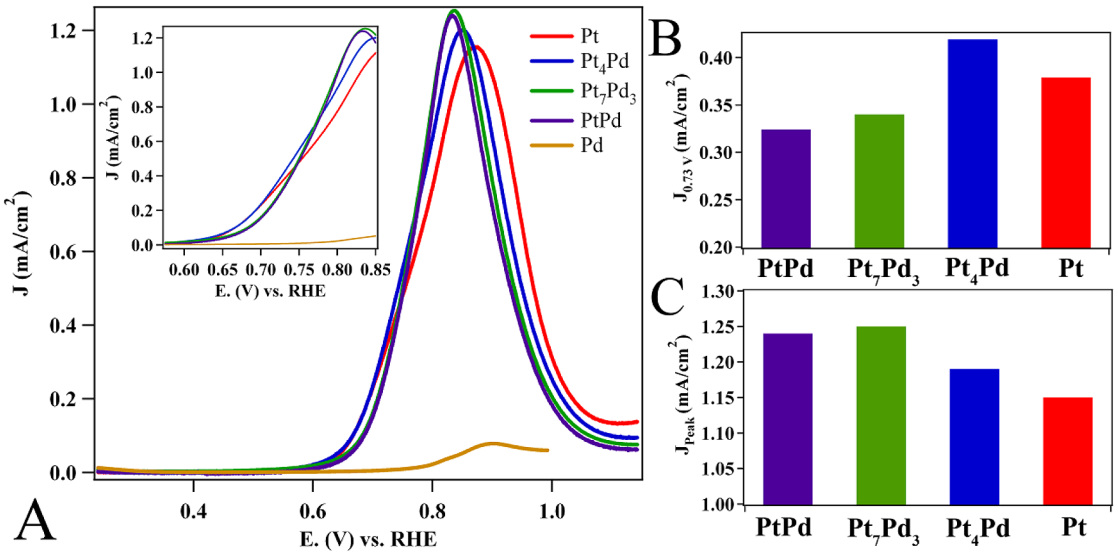

Figure 2. Representative LSVs obtained from various $Pt_{1-x}Pd_x$ NWs, including elemental Pt and Pd NWs, in 0.1 M methanol (A) with the onset region of the LSVs highlighted in the inset. The MOR kinetic current densities measured in the onset region at 0.73 V (B) and at the peak of the LSV (C) as a function of NW composition.

are expected to initiate methanol adsorption and oxidation at lower potentials, as compared with Pd active sites alone.[4,35] Although the Pt and Pt_4Pd NWs gave rise to comparable performances near the onset potential of ~0.63 V, a careful inspection of the onset region of the LSV (inset to Figure 2A) showed that the activity of the Pt_4Pd NWs exceeded that of the Pt NWs beyond ~0.72 V. To quantitatively explore their behavior in the onset region, the specific MOR activity of the various $Pt_{1-x}Pd_x$ NWs at 0.73 V was plotted with respect to NW composition in Figure 2B. On this basis, a volcano-type dependence in the specific MOR activity was noted in the onset region as a function of chemical composition with Pt_4Pd, yielding an optimum activity of 0.42 mA/cm^2.

Interestingly, the Pd-rich PtPd NWs and Pt_7Pd_3NWs displayed enhanced behavior in the peak region of the LSV and maintained peak potentials of 833 mV and 836 mV, respectively. These values are considerably lower than the corresponding peak potentials for the Pt_4Pd NWs and the Pt NWs, which were measured at 850 and 871 mV, respectively. In addition, the PtPd and Pt_7Pd_3 NWs possessed specific activities at the peak of the LSV (Figure 2C) of 1.24 and 1.25 mA/cm^2, respectively, which maintain a small but measurable enhancement with respect to those of the corresponding Pt_4Pd (1.19 mA/cm^2) and Pt NWs (1.15 mA/cm^2). Collectively, it is important to highlight that the performance of the composition-controlled $Pt_{1-x}Pd_x$ NW samples are all significantly enhanced beyond the activity measured for commercial Pt NP/C, thereby further reinforcing the intrinsic advantages of the 1D structural motif. We also note that the elemental Pd NWs evinced minimal MOR activity, which demonstrates that the enhanced performance emerges only with the bimetallic NW compositions. Thus, the observed composition-dependent behavior demonstrates that the addition of Pd content in $Pt_{1-x}Pd_x$ NWs within a finite composition regime can significantly and measurably improve the catalytic performance in both the onset region and the peak region of the LSV.

In the recent literature, the origin of the enhanced performance in nanostructured $Pt_{1-x}M_x$ (M = Pd or Au) alloys has been attributed to the incorporation of either Pd or Au into the bimetallic alloy. However, there has been a considerable debate regarding the origin of enhancement.[34,47−54] Specifically, it has been suggested by some in the community that the promoting effect of the Pd is a result of a surface-mediated bifunctional effect in a manner analogous to what has been found with $Pt_{1-x}Ru_x$ alloys. In the case of a bifunctional effect, the oxophilic Pd sites are expected to increase the coverage of adsorbed oxygen species at low potentials, thereby contributing to increased CO tolerance.[50]

To examine the likelihood of this reasonable scenario, we have methodically probed the relative interaction of the NW surface with adsorbed oxygen and CO species as a function of NW composition, utilizing both CV and CO stripping experiments. In a previous report, the relative onset of the characteristic surface oxide formation (e.g., adsorbed O and OH) feature was examined in the CV as a function of NW composition.[16] Although a shift in the onset of that oxide feature has been noted with increased Pd content, the onset of oxide formation in the PtPd NWs remains above 0.6 V.[16] The high onset of surface oxidation in these bimetallic NWs, despite the incorporation of Pd, provides strong evidence that the Pd itself does not contribute significantly to CO oxidation at potentials relevant to the onset of the MOR process, namely 0.5−0.6 V.

Using $Pt_{1-x}Ru_x$ alloys as a ubiquitous example of a catalyst that follows a bifunctional process, the addition of Ru to the $Pt_{1-x}Ru_x$ alloy promotes better CO oxidation kinetics, and there is an observed shift in the CO stripping peak to lower potentials as Ru content is increased to 30%. In this case, however, the CO stripping voltammograms obtained from our $Pt_{1-x}Pd_x$ NWs (Figure 3A) highlight a contrasting trend, wherein the stripping peak potential increased from 744 mV in Pt NWs to 819 mV as the Pd content was correspondingly increased to 50% in the $Pt_{1-x}Pd_x$ NWs. In fact, a plot of the CO stripping peak potential with respect to NW composition, shown in Supporting Information Figure S1, clearly illustrates that the CO stripping peak potential increases with increasing Pd content. Thus, the collective CV and CO stripping results yield strong evidence that the origin of the enhancement does not arise from a bifunctional effect, since the addition of the Pd active sites does not appear to contribute either to increased

dx.doi.org/10.1021/cs400380t | ACS Catal. 2013, 3, 2031−2040

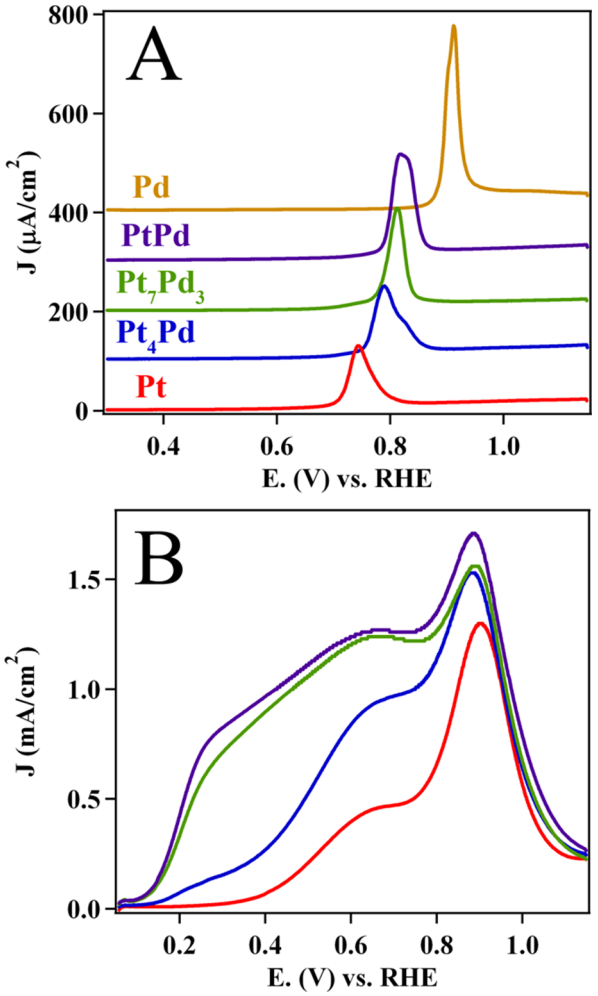

Figure 3. The composition-dependent electrocatalytic behavior toward CO stripping (A) and formic acid oxidation (B) in $Pt_{1-x}Pd_x$ NWs.

coverage of adsorbed oxygen species or to lower CO stripping peak potentials.

By contrast with the proposed bifunctional mechanism, other experimental[52,55] and first-principles[53,54] results have suggested that the enhancement in bimetallic surface alloys can be attributed to a change in the mechanism of MOR. Specifically, it is believed that in elemental Pt, the formation of the CO intermediate occurs readily via a so-called "indirect pathway" because of the presence of an abundance of Pt−Pt pair sites that catalyze the formation of CO. However, both bimetallic PtPd and PtAu alloys are believed to favor a direct oxidation or "CO-free pathway," since there are fewer Pt atoms and fewer Pt-pair sites present at the catalytic interface.[52] Moreover, a rational examination of the electronic properties associated with the bimetallic alloys of PtAu and PtPd by means of first-principles calculations has shown that the incorporation of Pd and Au in these structures can promote the selective formation of a formate ($HCOO^-$) intermediate, as opposed to CO.[53,54]

To purposely investigate this possibility, we have probed the formic acid oxidation performance so as to analyze the composition-dependent reactivity toward this intermediate. The study of formic acid oxidation is uniquely advantageous, since it represents a key intermediate in the MOR pathway and, more importantly, the oxidation of formic acid can serve as a useful probe for determining if either an indirect or direct CO-free oxidation pathway is favored.[55] Examination of the formic acid oxidation LSV (Figure 3B) for the elemental Pt NWs has led to an onset at ∼300 mV with a characteristic peak at ∼900 mV, which is consistent with prior reports for elemental Pt.[55,56] The peak at ∼900 mV is believed to be associated with the indirect oxidation of formic acid, thereby leading to a CO intermediate.[55] Interestingly, as the Pd content is increased in the $Pt_{1-x}Pd_x$ NWs to 50%, the onset for formic acid oxidation is shifted to ∼100 mV, and this process is accompanied by a considerable increase in the oxidation current in the 0.1−0.6 V range. On the basis of prior reports,[55,57] the increased formic acid oxidation at potentials below 0.6 V is consistent with the oxidation of formic acid via a direct CO-free pathway. Thus, it is apparent that the enhancement in the bimetallic $Pt_{1-x}Pd_x$ NWs may come about as a result of a modification of the traditionally expected oxidation pathway, due to the presence of fewer Pt−Pt pair sites at the catalytic interface, particularly when the Pd composition has been increased to 50%. Notwithstanding, the significant and clearly measurable improvements in both the methanol and formic acid oxidation performance have conclusively demonstrated the importance of tailoring chemical composition to provide for enhanced electrocatalytic activity in 1D nanostructures.

3.3. Stability of ORR Performance in $Pt_{1-x}Pd_x$ NWs in the Presence of Methanol. In addition to studying the performance of $Pt_{1-x}Pd_x$ alloy NWs toward MOR, we examined the stability of ORR performance in the presence of methanol. The goal in this case was to gain fundamental insights into the potential application of $Pt_{1-x}Pd_x$ alloy NWs as effective methanol-tolerant cathode electrocatalysts. In a functional DMFC, the rate of methanol crossover is dependent upon a variety of operating conditions, such as the concentration of the methanol in the anode, the fuel feed pressure, the relative humidity, and the chemistry of the PEM.[37] Thus, it is difficult to characterize the concentration of methanol within the cathode half-cell during operation in practical DMFC devices. Herein, we simulated the methanol crossover effect by purposefully adding in methanol into the 0.1 M $HClO_4$ electrolyte at concentrations ranging from 1 to 4 mM and measuring the corresponding ORR activity. This concentration regime is uniquely advantageous, since it is potentially higher than the actual methanol concentration within a practical DMFC, thereby representing a possible, realistic worst-case scenario while at the same time also enabling the accurate determination of specific ORR activity.

The polarization curves obtained in 0, 1, 2, 3, and 4 mM methanol are shown in Figure 4A−D for the Pt, Pt_4Pd, Pt_7Pd_3, and PtPd NWs, respectively. In all cases, the addition of methanol into the electrolyte medium results in a measurable positive deflection of the current in the polarization curves between 0.6 and 0.9 V, especially when compared with the polarization curve obtained in pure 0.1 M $HClO_4$. This deflection in the polarization curve increases with increasing methanol concentration and is consistent with the overlapping oxygen reduction and methanol oxidation processes occurring in this potential window. Careful inspection of the onset region for each set of polarization curves (insets to Figure 4A−D) also highlights a measurable decline in the current density in the region of the curve that follows the onset of ORR kinetics.

The ratio of the calculated specific ORR activity (e.g., J_K [MeOH]) in the presence of methanol was normalized to the specific ORR activity measured in pure electrolyte (J_K) so as to provide a quantitative insight into the relative decline in specific

dx.doi.org/10.1021/cs400380t | ACS Catal. 2013, 3, 2031−2040

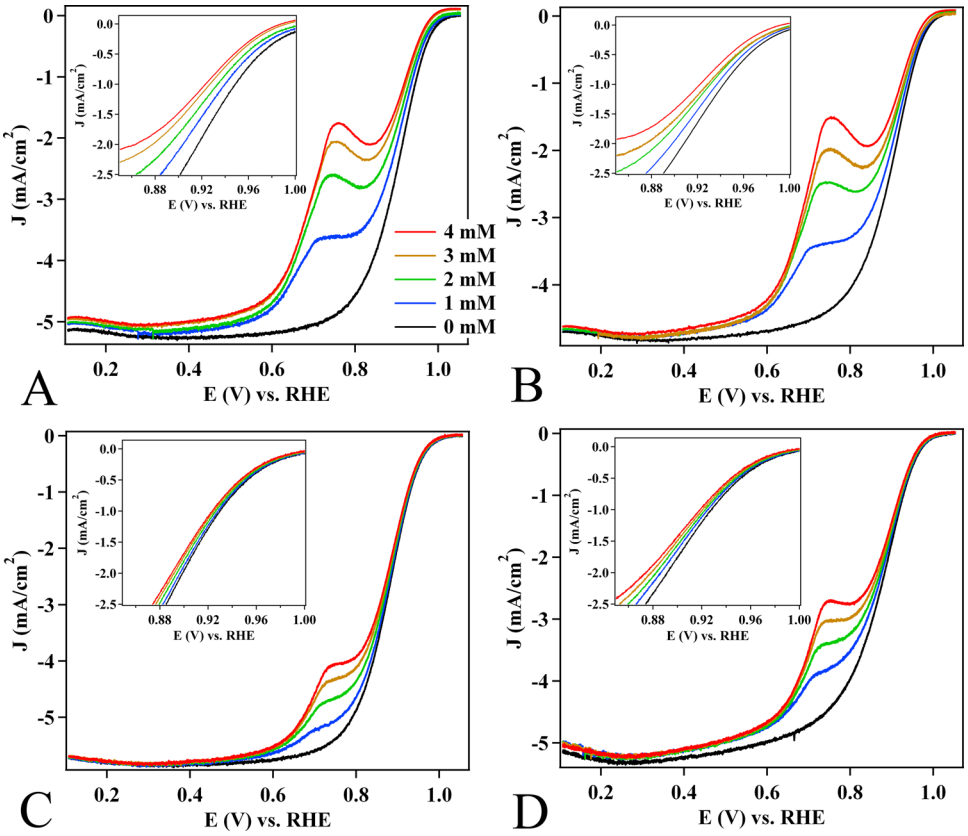

Figure 4. The stability of ORR performance in $Pt_{1-x}Pd_x$ NWs in the presence of methanol. The polarization curves obtained from Pt (A), Pt_4Pd (B), Pt_7Pd_3 (C), and PtPd (D) NWs are shown with methanol concentrations ranging from 0 to 4 mM. The onset regions of the polarization curves for each $Pt_{1-x}Pd_x$ NW are also shown as the corresponding insets.

activity as a function of methanol concentration. The resulting methanol tolerance curves are shown in Figure 5 for the $Pt_{1-x}Pd_x$ NWs. The elemental Pd NWs maintained the highest stability in the presence of methanol with a loss of only ~6% of the activity in 4 mM methanol. This result was important, since the Pd NWs maintained essentially no activity toward methanol oxidation (Figures 2A and S2A) by comparison with the Pt NWs. In terms of the $Pt_{1-x}Pd_x$ NWs, the increased Pt content in the alloy nanowires led to a lower overall methanol tolerance as compared with the elemental Pd NWs themselves. It is worth noting that the elemental Pt NWs maintained the lowest stability and retained only 43% of their initial activity in the presence of 4 mM methanol.

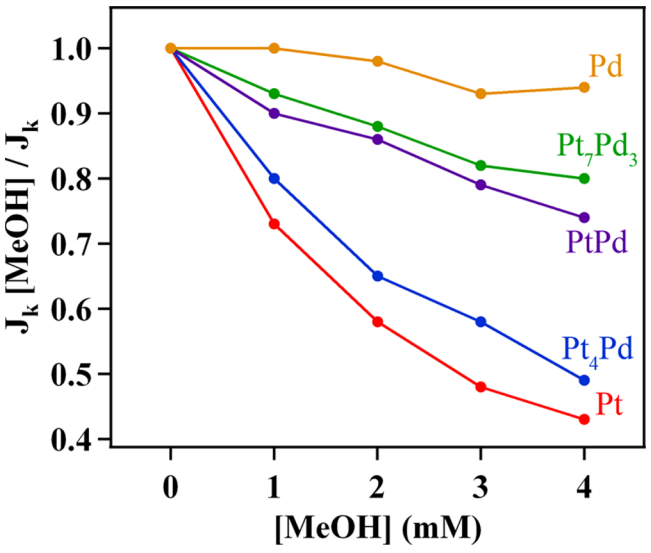

Figure 5. A plot of the ratio of the specific activity, measured in the presence of methanol (J_K [MeOH], 0–4 mM), with respect to the specific activity, measured in pure 0.1 M $HClO_4$ electrolyte (J_K), as a function of methanol concentration for the $Pt_{1-x}Pd_x$ NWs.

Interestingly, the performance of the $Pt_{1-x}Pd_x$ NWs did not trend linearly with respect to increasing Pt content, and in fact, a volcano-type dependence was observed with the Pt_7Pd_3 NWs found to maintain the best ORR stability in the presence of methanol. Specifically, the Pt_7Pd_3 NWs preserved 80% of their initial activity, which was noticeably and measurably enhanced with respect to both PtPd (74%) and, especially, Pt_4Pd (49%). Recently, analogous studies of nanoparticulate $Pt_{1-x}Pd_x$ catalysts have demonstrated a strong inverse correlation between MOR activity and the stability of ORR performance in the presence of methanol.[39−43] The observed trend in NP analogues is not surprising, since highly active MOR catalysts are expected to be more sensitive to the presence of methanol when operating as ORR catalysts. However, we have demonstrated herein that simultaneously and carefully tailoring both morphology and chemical composition in $Pt_{1-x}Pd_x$ NWs can lead to an optimal chemical composition (e.g., Pt_7Pd_3), which is not only highly active toward MOR but also practically stable as an ORR catalyst in the presence of methanol. This observation is consistent with the notion that the added Pd content likely contributes to a different reaction pathway in the

dx.doi.org/10.1021/cs400380t | ACS Catal. 2013, 3, 2031−2040

case of the MOR, as opposed to merely increasing the CO tolerance.

3.4. Toward a Pt-Free Methanol Tolerant Electrocatalyst: Stability of ORR Performance in Highly-Active Pd_9Au NWs in the Presence of Methanol. Although the $Pt_{1-x}Pd_x$ NWs represent a key system with respect to insights into the composition-dependent behavior in the presence of methanol, we have recently developed Pd_9Au NWs as a novel Pt-free electrocatalyst that maintains outstanding performance toward ORR.[16] In a prior study, we have demonstrated this system to be uniquely advantageous, since the addition of 10% gold, forming a bimetallic alloy, results in a specific activity of 0.45 mA/cm^2 that is nearly 2-fold higher than that of commercial Pt NP/C (0.2 mA/cm^2) and of elemental Pd NW analogues (0.21 mA/cm^2). However, there have been no reports, to the best of our knowledge, investigating the stability of ORR activity in the presence of methanol. In this section, we have performed a concise investigation of the stability of ORR performance in the presence of methanol for Pt-free Pd and Pd_9Au NWs by comparison with elemental Pt NWs.

The methanol oxidation performance of the Pd_9Au NWs was characterized by obtaining a LSV in 0.1 M methanol supported in 0.1 M $HClO_4$. The measured LSV (Supporting Information Figure S2B) shows a minimal MOR peak activity of 0.08 mA/cm^2 by comparison with that of the Pt NWs (1.16 mA/cm^2) and is analogous to the LSV, obtained for elemental Pd NWs. This encouraging result suggests that the Pt-free, Pd_9Au NWs maintained a high degree of electrochemical stability, even in the presence of up to 100 mM methanol. To quantitatively probe the ORR stability in the presence of methanol, polarization curves were obtained from the Pd_9Au NWs in 0−4 mM methanol. Interestingly, the presence of methanol yields minimal effect on the measured polarization curves shown in Figure 6A, which starkly contrasts with the results obtained with the bimetallic $Pt_{1-x}Pd_x$ NWs and elemental Pt NWs (Figure 4). Given the high methanol tolerance of the Pd_9Au NWs, the stability of ORR performance in methanol (Figure 6B) has been compared with commercial Pt NP/C, Pt NWs, and Pd NWs, respectively. Of special interest, the Pd_9Au NWs retained 88% of their initial activity in the presence of 4 mM methanol, a result demonstrating considerable enhancement with respect to both conventional Pt NP/C (79%) and elemental Pt NWs (43%).

From a practical perspective, the measured specific activity of the Pd_9Au NWs, Pt NWs, commercial Pt NP/C, and Pd NWs is shown before and after the addition of 4 mM methanol in Figure 6C. In pure 0.1 M $HClO_4$, the Pt NWs maintained a demonstrably higher specific activity (0.76 mA/cm^2) as compared with Pd_9Au NWs (0.48 mA/cm^2), Pd NWs (0.32 mA/cm^2), and commercial Pt NP/C (0.30 mA/cm^2). In the presence of 4 mM methanol, the high methanol tolerance of the Pd_9Au NWs was highlighted, and these nanowires yielded a specific activity of 0.42 mA/cm^2, a value that is considerably enhanced beyond that of the elemental Pt NWs (0.32 mA/cm^2). Collectively, these results have demonstrated the intrinsic advantages of as-synthesized Pd_9Au and Pd NWs, since they are both highly active and also tolerant to methanol as ORR electrocatalysts.

At methanol concentrations below 4 mM, we find that Pd and Pd_9Au NWs maintain essentially similar trends in ORR stability and mutually outperform Pt analogues (Figure 6B); however, an interesting trend emerges in Pd and Pd_9Au NWs when the performance is studied in methanol concentrations of

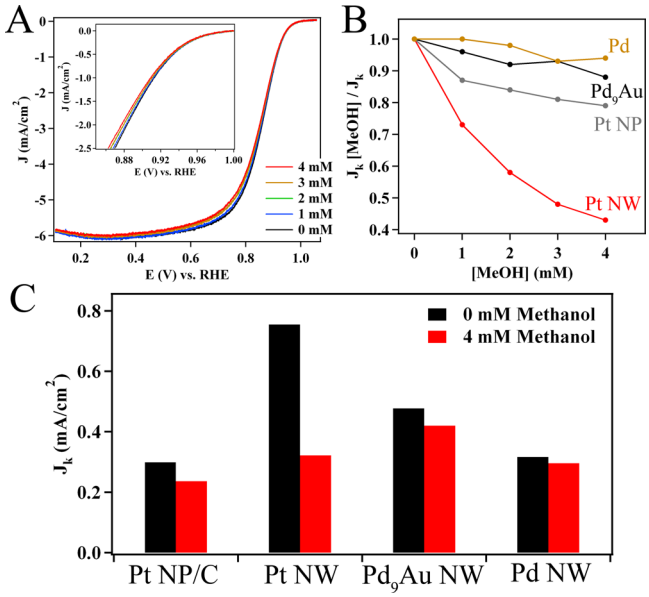

Figure 6. The stability of ORR performance in highly active, Pt-free, Pd_9Au NWs. Polarization curves obtained from Pd_9Au NWs are shown with the methanol concentration, ranging from 0 to 4 mM. A plot of the ratio of the specific activity measured in the presence of methanol (J_K [MeOH]) with respect to the specific activity measured in pure electrolyte (J_K) as a function of methanol concentration (B) for the Pd_9Au NWs, Pt NWs, Pd NWs, and commercial Pt NP/C. In C, a bar graph is shown that depicts the measured specific activity of the various catalysts in pure 0.1 M $HClO_4$ as well as in 4 mM methanol supported in 0.1 M $HClO_4$.

up to 100 mM. Polarization curves obtained from Pd_9Au and Pd NWs in 25−100 mM methanol in 0.1 M $HClO_4$ (Figure 7) reveal that the measured half-wave potential decreased by approximately 35 mV and 15 mV, respectively. In the context of the specific activity (Supporting Information Figure S3), the Pd NWs retained 87% of their initial activity, which was a noteworthy improvement over that of Pd_9Au NWs (57%). The lower methanol tolerance of the Pd_9Au NWs, by comparison with the elemental Pd NWs, may be attributed to the effects of the gold dopant in the homogeneous $Pd_{1-x}Au_x$ alloy.

According to the relevant literature regarding $Pd_{1-x}Au_x$ alloys, the addition of Au into the face-centered cubic Pd framework (i) results in a slight expansion of the Pd lattice (3.89 Å), thereby rendering the lattice parameter of Pd_9Au (3.91 Å) closer to that of Pt (3.92 Å), and (ii) increases the relative number of electrons in the Pd d-band.[58,59] These mutually advantageous effects cause the Pd_9Au alloys to be more active toward ORR, since their structural and electronic properties are closer to those of more active Pt nanostructures.[15,16] However, on the basis of Nørskov and Hammer theory,[46,60,61] the increased number of electrons in the d-band is also expected to strengthen the d-band-to-π^* overlap of the $Pd_{1-x}Au_x$ NWs with adsorbed CO, by comparison with an elemental analogue. This increase in the surface adsorption strength of the CO is expected to render the Pd_9Au NW more susceptible to CO poisoning by comparison with elemental Pd NWs when operating as an ORR catalyst in the presence of methanol. Collectively, we believe that these data support the observed trend in the activity loss in the Pd_9Au and Pd NWs at methanol concentrations above 25 mM.

dx.doi.org/10.1021/cs400380t | ACS Catal. 2013, 3, 2031−2040

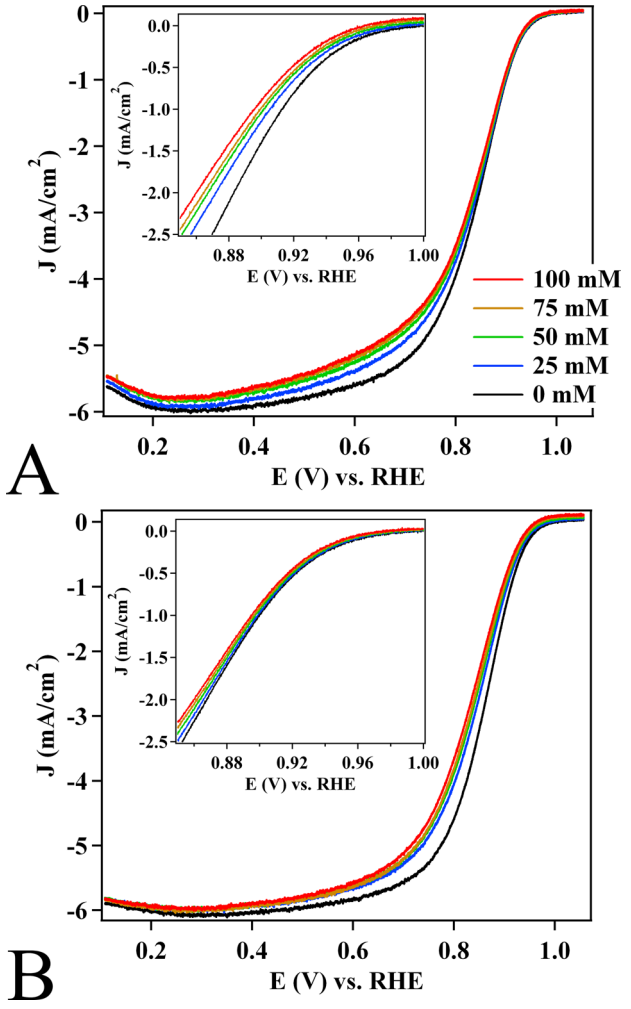

Figure 7. Polarization curves obtained from Pd NWs (A) and Pd_9Au NWs (B) in 0.1 M $HClO_4$ with increasing methanol concentration of 25, 50, 75, and 100 mM, respectively.

4. CONCLUSIONS

Recently, work associated with developing electrocatalysts for direct alcohol fuel cells have focused on resolving two key and significant challenges: (i) improving the electrocatalytic performance of anode catalysts toward the oxidation of SOMs and (ii) developing cathode catalysts with high ORR activity in the presence of measurable concentrations of SOMs. In this report, we have explored these two important concerns in the context of a new class of 1D palladium-based nanowires, wherein the physicochemical properties of the nanowires, such as morphology and chemical composition, have been rationally tailored for enhanced performance.

In the context of addressing the first technical challenge, we have examined the morphology and composition-dependent performance of $Pt_{1-x}Pd_x$ NWs toward MOR. Elemental Pt NWs were found to possess a significant morphology-dependent enhancement of nearly 3-fold in terms of peak MOR specific activity over commercial Pt NP/C. Drawing upon the intrinsic advantages associated with 1D nanowires, we have tailored the chemical composition of $Pt_{1-x}Pd_x$ to measurably increase the MOR kinetics in both the onset and peak regions of the LSV. In the context of the second technical challenge, we have explored the stability of ORR performance in the presence of measurable concentrations of methanol so as to simulate the effects of methanol crossover in a DMFC and to examine the corresponding influence of the NW morphology upon stability. A distinctive volcano-type dependence has been noted with respect to chemical composition in the $Pt_{1-x}Pd_x$ NWs, and on the basis of the MOR activities and methanol tolerant ORR behavior, Pt_7Pd_3 NWs have been highlighted as a particularly intriguing catalyst system with optimized chemical composition and morphology.

From the perspective of dealing with real-world limitations associated with practical fuel cells, we have also analyzed the methanol tolerance in Pd_9Au NWs, which represent a highly active, durable Pt-free alternative to traditional Pt-based nanostructured catalysts. In effect, the Pd_9Au NWs maintained 88% of their intrinsic activity in the presence of 4 mM methanol, thereby giving rise to a significantly higher stability as compared with Pt NWs (43%) and Pt NP/C (79%), respectively. In fact, we have demonstrated in this report that completely Pd-based, Pt-free NW architectures can outperform analogous Pt-based nanostructures in the presence of methanol, which is a very promising result in the context of developing novel multifunctional catalyst architectures.

■ ASSOCIATED CONTENT

Supporting Information

Additional electrochemical characterization data of the NWs, including MOR catalysis results and ORR stability in the presence of methanol, are presented. This material is available free of charge via the Internet at http://pubs.acs.org

■ AUTHOR INFORMATION

Corresponding Author

*E-mail: stanislaus.wong@stonybrook.edu, sswong@bnl.gov.

Notes

The authors declare no competing financial interest.

■ ACKNOWLEDGMENTS

Research (including support for C.K. and S.S.W. and electrochemical experiments) was supported by the U.S. Department of Energy, Basic Energy Sciences, Materials Sciences and Engineering Division. We also thank R. R. Adzic and M. B. Vukmirovic for use of their facilities and assistance with electrochemical measurements at Brookhaven National Laboratory, which is supported by the U.S. Department of Energy under Contract No. DE-AC02-98CH10886.

■ REFERENCES

(1) Morozan, A.; Jousselme, B.; Palacin, S. *Energy Environ. Sci.* **2011**, *4*, 1238−1254.
(2) Antolini, E.; Perez, J. *J. Mater. Sci.* **2011**, *46*, 1−23.
(3) Koenigsmann, C.; Scofield, M. E.; Liu, H.; Wong, S. S. *J. Phys. Chem. Lett.* **2012**, *3*, 3385−3398.
(4) Koenigsmann, C.; Wong, S. S. *Energy Environ. Sci.* **2011**, *4*, 1161−1176.
(5) Watanabe, M.; Tryk, D. A.; Wakisaka, M.; Yano, H.; Uchida, H. *Electrochim. Acta* **2012**, *84*, 187−201.
(6) Rabis, A.; Rodriguez, P.; Schmidt, T. J. *ACS Catal.* **2012**, *2*, 864−890.
(7) Wang, C.; Ma, D.; Bao, X. *J. Phys. Chem. C* **2008**, *112*, 17596−17602.
(8) Beier, M. J.; Kleist, W.; Wharmby, M. T.; Kissner, R.; Kimmerle, B.; Wright, P. A.; Grunwaldt, J.-D.; Baiker, A. *Chem.—Eur. J.* **2012**, *18*, 887−898.
(9) Koenigsmann, C.; Zhou, W.-p.; Adzic, R. R.; Sutter, E.; Wong, S. S. *Nano Lett.* **2010**, *10*, 2806−2811.

(10) Zhou, W.-P.; Li, M.; Koenigsmann, C.; Ma, C.; Wong, S. S.; Adzic, R. R. *Electrochim. Acta* **2011**, *56*, 9824−9830.
(11) Wang, S.; Jiang, S. P.; Wang, X.; Guo, J. *Electrochim. Acta* **2011**, *56*, 1563−1569.
(12) Matanović, I.; Kent, P. R. C.; Garzon, F. H.; Henson, N. J. *J. Phys. Chem. C* **2012**, *116*, 16499−16510.
(13) Koenigsmann, C.; Santulli, A. C.; Gong, K.; Vukmirovic, M. B.; Zhou, W.-p.; Sutter, E.; Wong, S. S.; Adzic, R. R. *J. Am. Chem. Soc.* **2011**, *133*, 9783−9795.
(14) Koenigsmann, C.; Santulli, A. C.; Sutter, E.; Wong, S. S. *ACS Nano* **2011**, *5*, 7471−7487.
(15) Koenigsmann, C.; Sutter, E.; Adzic, R. R.; Wong, S. S. *J. Phys. Chem. C* **2012**, *116*, 15297−15306.
(16) Koenigsmann, C.; Sutter, E.; Chiesa, T. A.; Adzic, R. R.; Wong, S. S. *Nano Lett.* **2012**, *12*, 2013−2020.
(17) Zhou, H.; Zhou, W.-p.; Adzic, R. R.; Wong, S. S. *J. Phys. Chem. C* **2009**, *113*, 5460−5466.
(18) Koenigsmann, C.; Tan, Z.; Peng, H.; Sutter, E.; Jacobskind, J.; Wong, S. S. *Isr. J. Chem.* **2012**, *52*, 1090−1103.
(19) Chen, Z.; Waje, M.; Li, W.; Yan, Y. *Angew. Chem., Int. Ed.* **2007**, *46*, 4060−4063.
(20) Liang, H.-W.; Cao, X.; Zhou, F.; Cui, C.-H.; Zhang, W.-J.; Yu, S.-H. *Adv. Mater.* **2011**, *23*, 1467−1471.
(21) Sun, S.; Jaouen, F.; Dodelet, J.-P. *Adv. Mater.* **2008**, *20*, 3900−3904.
(22) Zhiyong, Z.; Li, M.; Wu, Z.; Li, W. *Nanotechnology* **2011**, *22*, 015602.
(23) Liu, L.; Pippel, E. *Angew. Chem., Int. Ed.* **2011**, *50*, 2729−2733.
(24) Xu, C.; Zhang, Y.; Wang, L.; Xu, L.; Bian, X.; Ma, H.; Ding, Y. *Chem. Mater.* **2009**, *21*, 3110−3116.
(25) Aricò, A. S.; Srinivasan, S.; Antonucci, V. *Fuel Cells* **2001**, *1*, 133−161.
(26) Chuan-Jian, Z.; Jin, L.; Bin, F.; Bridgid, N. W.; Peter, N. N.; Rameshwori, L.; Jun, Y. *Nanotechnology* **2010**, *21*, 062001.
(27) Wee, J.-H.; Lee, K.-Y. *J. Power Sources* **2006**, *157*, 128−135.
(28) Liu, H.; Song, C.; Zhang, L.; Zhang, J.; Wang, H.; Wilkinson, D. P. *J. Power Sources* **2006**, *155*, 95−110.
(29) Rauber, M.; Alber, I.; Müller, S.; Neumann, R.; Picht, O.; Roth, C.; Schökel, A.; Toimil-Molares, M. E.; Ensinger, W. *Nano Lett.* **2011**, *11*, 2304−2310.
(30) Wang, S.; Wang, X.; Jiang, S. P. *Nanotechnology* **2008**, *19*, 455602.
(31) Maksimuk, S.; Yang, S.; Peng, Z.; Yang, H. *J. Am. Chem. Soc.* **2007**, *129*, 8684−8685.
(32) Yuan, Q.; Zhou, Z.; Zhuang, J.; Wang, X. *Chem. Mater.* **2010**, *22*, 2395−2402.
(33) Guo, S.; Zhang, S.; Sun, X.; Sun, S. *J. Am. Chem. Soc.* **2011**, *133*, 15354−15357.
(34) Cui, C.-H.; Yu, J.-W.; Li, H.-H.; Gao, M.-R.; Liang, H.-W.; Yu, S.-H. *ACS Nano* **2011**, *5*, 4211−4218.
(35) Zhu, C.; Guo, S.; Dong, S. *Adv. Mater.* **2012**, *24*, 2326−2331.
(36) Niu, Z.; Wang, D.; Yu, R.; Peng, Q.; Li, Y. *Chem. Sci.* **2012**, *3*, 1925−1929.
(37) Heinzel, A.; Barragán, V. M. *J. Power Sources* **1999**, *84*, 70−74.
(38) Antolini, E.; Lopes, T.; Gonzalez, E. R. *J. Alloys Compd.* **2008**, *461*, 253−262.
(39) He, W.; Liu, J.; Qiao, Y.; Zou, Z.; Zhang, X.; Akins, D. L.; Yang, H. *J. Power Sources* **2010**, *195*, 1046−1050.
(40) Lee, C.-L.; Chiou, H.-P. *Appl. Catal., B* **2012**, *117*−*118*, 204−211.
(41) Lee, C.-L.; Chiou, H.-P.; Wu, S.-C.; Wu, C.-C. *Electrochim. Acta* **2010**, *56*, 687−692.
(42) Wang, W. M.; Li, Z. L.; Zou, Z.; Yang, H.; Feng, S. *ECS Transactions* **2008**, *16*, 613−619.
(43) Yang, J.; Zhou, W.; Cheng, C. H.; Lee, J. Y.; Liu, Z. *ACS Appl. Mater. Interfaces* **2009**, *2*, 119−126.
(44) Garsany, Y.; Baturina, O. A.; Swider-Lyons, K. E.; Kocha, S. S. *Anal. Chem.* **2010**, *82*, 6321−6328.
(45) Hamnett, A. In *Interfacial Electrochemistry: Theory, Experiment and Applications*; Wieckowski, A., Ed.; Marcel Dekker: New York, NY, 1999, p 843−879.
(46) Feibelman, P. J.; Hammer, B.; Nørskov, J. K.; Wagner, F.; Scheffler, M.; Stumpf, R.; Watwe, R.; Dumesic, J. *J. Phys. Chem. B* **2000**, *105*, 4018−4025.
(47) Mott, D.; Luo, J.; Njoki, P. N.; Lin, Y.; Wang, L.; Zhong, C.-J. *Catal. Today* **2007**, *122*, 378−385.
(48) Luo, J.; Njoki, P. N.; Lin, Y.; Mott, D.; Wang, L.; Zhong, C.-J. *Langmuir* **2006**, *22*, 2892−2898.
(49) Yang, L.; Yang, W.; Cai, Q. *J. Phys. Chem. C* **2007**, *111*, 16613−16617.
(50) Liu, Y.; Chi, M.; Mazumder, V.; More, K. L.; Soled, S.; Henao, J. D.; Sun, S. *Chem. Mater.* **2011**, *23*, 4199−4203.
(51) Choi, J.-H.; Park, K.-W.; Park, I.-S.; Kim, K.; Lee, J.-S.; Sung, Y.-E. *J. Electrochem. Soc.* **2006**, *153*, A1812−A1817.
(52) Yin, M.; Huang, Y.; Liang, L.; Liao, J.; Liu, C.; Xing, W. *Chem. Commun.* **2011**, *47*, 8172−8174.
(53) Zhong, W.; Liu, Y.; Zhang, D. *J. Phys. Chem. C* **2012**, *116*, 2994−3000.
(54) Yuan, D.; Gong, X.; Wu, R. *J. Chem. Phys.* **2008**, *128*, 064706−064705.
(55) Cui, C.-H.; Li, H.-H.; Cong, H.-P.; Yu, S.-H.; Tao, F. *Chem. Commun.* **2012**, *48*, 12062−12064.
(56) Zhang, S.; Shao, Y.; Liao, H.-g.; Liu, J.; Aksay, I. A.; Yin, G.; Lin, Y. *Chem. Mater.* **2011**, *23*, 1079−1081.
(57) Vidal-Iglesias, F. J.; Solla-Gullón, J.; Herrero, E.; Aldaz, A.; Feliu, J. M. *Angew. Chem., Int. Ed.* **2010**, *49*, 6998−7001.
(58) Damjanovic, A.; Brusić, V. *Electrochim. Acta* **1967**, *12*, 1171−1184.
(59) Damjanovic, A.; Brusic, V.; Bockris, J. O. M. *J. Phys. Chem.* **1967**, *71*, 2741−2742.
(60) Greeley, J.; Norskov, J. K. *J. Phys. Chem. C* **2009**, *113*, 4932−4939.
(61) Nørskov, J. K.; Rossmeisl, J.; Logadottir, A.; Lindqvist, L.; Kitchin, J. R.; Bligaard, T.; Jonsson, H. *J. Phys. Chem. B* **2004**, *108*, 17886−17892.